HHS Public Access

Author manuscript

Adv Healthc Mater. Author manuscript; available in PMC 2022 August 01.

Published in final edited form as:

Adv Healthc Mater. 2021 August ; 10(16): e2002150. doi:10.1002/adhm.202002150.

Nanoparticle and Biomolecule Surface Modification Synergistically Increases Neural Electrode Recording Yield and Minimizes Inflammatory Host Response

Kevin M. Woeppel[1,2], **Xinyan Tracy Cui**[1,2,3]

[1]University of Pittsburgh, Department of Bioengineering

[2]Center for the Neural basis of Cognition

[3]McGowan Institute for Regenerative Medicine

Abstract

Due to their ability to interface with neural tissues, neural electrodes are the key tool used for neurophysiological studies, electrochemical detection, brain computer interfacing, and countless neuromodulation therapies and diagnostic procedures. However, the long-term applications of neural electrodes are limited by the inflammatory host tissue response, decreasing detectable electrical signals, and insulating the device from the native chemical environment. Surface modification methods have been proposed to limit these detrimental responses, but each has their own limitations. Here, we present a combinatorial approach towards creating a stable interface between the electrode and host tissues. First, a thiolated nanoparticle (TNP) coating was utilized to increase the surface area and roughness. Next, the neural adhesion molecule L1 was immobilized to the nanoparticle modified substrate. *In vitro*, the combined nanotopographical and bioactive modifications (TNP+L1) elevated the bioactivity of L1, which was maintained for 28 days. *In vivo*, TNP+L1 modification improved the recording performance of the neural electrode arrays compared to TNP or L1 modification alone. Post-mortem histology revealed greater neural cell density around the TNP+L1 coating while eliminating any inflammatory microglial encapsulation after four weeks. These results demonstrate that nanotopographical and bioactive modifications synergistically produced a seamless neural tissue interface for chronic neural implants.

Keywords

Neural Electrode; Bioactive Coating; Electrophysiology; Surface Modification; Nanoparticle

1. Introduction

Neural electrodes are devices designed to detect the electrical fluctuations between communicating neurons and provide precise electrical inputs to the nervous system. The unparalleled signal resolution of these devices is a key component of brain-computer interfaces, a promising therapy for people with paralysis.[1–3] Additionally, these minuscule

xic11@pitt.edu .

electrodes are employed for neurological investigation[4, 5] or real-time electrochemical detection of compounds in the tissue.[6–9] However, the implantation of the device into the tissues elicits an inflammatory reaction which can result in encapsulation of the device by glia and loss or degeneration of neurons from the site of implantation.[10, 11] These reactions may compromise the neural recording/stimulation ability, while also hampering electrochemical detection by blocking the diffusion of compounds to the sensing surface.[7] Control over these detrimental inflammatory reactions is vital to ensuring stable chronic implant functions.

Many strategies have been investigated for minimizing the inflammatory host tissue response to implants, including reducing implant size,[12] increasing flexibility,[13–16] surface modification, and administration of anti-inflammatory compounds.[17–20] Among these, surface modification holds great promises in that it only minimally modifies the implant at the surface where it interacts directly with the biological tissue, without affecting mechanical and electrical functionality and durability of the implant. Bioactive coatings are one type of surface modification. Molecules such as proteins, peptides, and therapeutic compounds are immobilized to the surface of the implants to disguise the electrode as a non-foreign material or control the tissue reactions after implantation. For example, catalytic antioxidants such as superoxide dismutase mimics (SODMs) that control inflammatory signaling by eliminating reactive oxygen and nitrogen species[20, 21] have been functionalized and immobilized on neural probe surface, and were found to lower inflammatory markers *in vivo* after 1 week of implantation.[21] Meanwhile, coatings derived from laminin or laminin peptides on the shank[22] or electrode sites[23–26] have been effective at increasing neuron adhesion to the device *in vitro* and decreasing glial encapsulation *in vivo*. L1, a neuron adhesion protein, has attracted our attention as an ideal candidate for neural electrode coating due to its ability to specifically promote neuron adhesion lowering fibroblast and astrocyte attachment *in vitro*,[27, 28] as well as the numerous evidence supporting the promotion of neural regeneration.[29–32] When bound to the neural electrode, L1 decreases microglia activation and astrogliosis, increases the number of neurons adjacent to the electrode and improves electrophysiological recording for up to 16 weeks.[11, 29, 33–35] While highly promising, bioactive coatings may have limitations stemming from their limited bioactive lifetimes and their binding being limited to the surface area of the electrode.

Another surface modification strategy for encouraging a healthy integration of the electrode and the host tissues is to tailor the surface micro and nano topography via different means of topographical modification and patterning. The effects of topographic modifications *in vitro* have been extensively studied. Neurons grown on topographically modified substrates were more viable[36], and had greater neurite outgrowth.[27, 37–39] Neuron differentiation and outgrowth can be affected by micro to nano geometries such as nanopillars,[40–42] nanofibers,[43, 44] and nanopores.[45, 46] Topography can also vary in organization, with aligned features encouraging more directional neuron outgrowth than random features.[43, 44] Further, micro-topographical changes alter glial cell phenotypes[47] with rougher surfaces decreasing glial cell activation *in vitro*.[45, 48] However, topographic modifications alone have not been shown to be sufficient at halting inflammation in response to neural electrode implantation *in vivo*.[49] In addition, while certain topographical modifications are

non-damaging[27] many require that the surface be etched or eroded,[37, 38, 48, 49] treatments that are likely to be incompatible with thinly insulated microelectrode devices.

The potential of synergistic effects of bioactive coatings and topographical modifications in producing stable chronic neural electrodes has been less explored. Topographical modifications can increase the surface area for modification, effectively increasing the number of binding sites. Recently, we have shown that the increase in binding sites increases the amount of immobilized bioactive molecules which leads to enhanced bioactivity.[27] Others have shown that proteins immobilized to nano-topographical surfaces are more stable than their soluble counterparts.[50]

Herein we developed and validated a nano-topographical bioactive neural electrode coating. First, we created a topographical modification by immobilizing thiol-functionalized silica nanoparticles (TNP) to the surface of silicon and glass substrates. Next, the TNP surface was covalently coated with the neural adhesion protein L1. We examined the bioactivity and stability of the coating *in vitro* with comparisons made to the L1 coated smooth surface without TNP. Finally, the TNP+L1 coating was applied to silicon based single shank electrode arrays to evaluate the synergistic effects of TNP and L1 on neural recording performance and tissue reactions *in vivo*.

2. Results

2.1 Nanoparticle characterization and Deposition

Nanoparticles were fabricated from tetraethylorthosilicate (TEOS) and mercaptopropyl trimethoxysilane (MTS) under basic conditions, as done in our prior work.[27] Particle deposition is predicated on the interaction between thiols, amines, and the hetero-crosslinker gamma-maleimidobutyryl-oxysuccinimide ester (GMBS), as shown in scheme 1. The deposition was monitored stepwise via water contact angle (WCA) and ellipsometry (Figure 1A), measuring changes in hydrophilicity and roughness respectively between steps. Substrates were first cleaned with acetone and isopropanol to remove larger contaminates, then activated under O_2 plasma. O_2 plasma treatment eliminated any organic contamination on these substrates, and also dramatically increased the hydrophilicity of the substrate with WCA decreased from 65.0° ± 5.3° to 11.3° ± 2.3° (mean ± SD). Next, aminopropyl triethoxysilane (APTES) was then reacted with the activated substrate, which was verified by the increase in WCA (61.9° ± 1.6°). The amine groups were then linked to the GMBS crosslinker, reducing the contact angle (40.6° ± 3.5°). Finally, the maleimide group on GMBS reacted with the TNP to covalently link the nanoparticles to the silicon or glass. The WCA significantly decreased after particle immobilization (13.1° ± 2.3°), while the RMS roughness of the substrate increased (78.6nm ±0.2nm). Nanoparticle distribution was then visualized under SEM (Figure 1B). Modification of the silicon substrate with TNP occurred uniformly across the substrate. TNP bound to each other, producing larger interconnected features with even greater roughness and surface area than would be expected from a single monolayer of nanoparticles.

2.2 Protein Binding and Binding Lifetime

The effect of surface topography on increasing protein bioactivity and stability was assessed via culture of primary cortical neurons (Figure 2). Glass coverslips were modified to display either thiol groups (smooth substrates) or nanoparticles (rough substrates). Smooth thiol modified substrates were produced by reacting activated glass substrates with MTS, mimicking the surface chemistry of rough substrates. Both smooth and rough samples were then reacted with GMBS followed by immobilization of L1 (see scheme in Figure 2A&B). WCA of the resulting TNP+L1 and smooth L1 surfaces were 57.4° ± 4.7° and 52.4° ± 2.6°. Smooth and nanoparticle modified coverslips coated with L1 were incubated in PBS at 37°C to examine the relative amounts of bound L1 and whether the L1 will detach from the substrate over time. We observed that there was a 75% increase in the amount of L1 bound to the TNP modified surface relative to the smooth surface prior to the incubation, indicating that more L1 was able to bind to the TNP modified surface. After incubation, the amount of L1 bound to the smooth surface decreased by 59.05% and 64.56% after one and four weeks, respectively. Conversely, the amount of L1 bound to the TNP modified surfaces was better retained, decreasing by 3.53% after one week and 15.23% after four weeks (Figure 2C).

2.3 Bioactivity of L1 and Bioactive Lifetime

Next, we examined the long-term bioactivity of L1 bound to smooth or rough substrates. Sets of L1 modified samples were soaked in PBS at 37°C for 3 days, 7 days, or 28 days to determine if the bioactivity of immobilized L1 decreases under physiologic conditions. Additional modified coverslips were created without protein modification to examine the effect of topography on neurite outgrowth. Primary neurons were cultured directly onto the substrates for 36 hours, followed by fixation and staining for β(III)-tubulin (neurons) and DAPI (nuclei). Topographical modification had a significant effect on neurite outgrowth, with an increase in the overall length of projections compared to a smooth surface without subsequent protein modification (Figure 2E). Meanwhile, L1 immobilization was advantageous regardless of surface topography, with significant increases in neurite outgrowth apparent on both smooth and rough substrates at early time points (Figure 2E). Overall, L1 modified rough substrates produced the highest neurite outgrowth of the test conditions. Furthermore, L1 was not stable on smooth substrates, with significant decreases in total neurite projections observed between the fresh and the 7 and 28 day time points. On the other hand, there was no observed decrease in neurite outgrowth for L1 modified rough substrates, regardless of incubation time (Figure 2F).

2.4 Electrical Properties and Electrophysiology Performance of Modified Electrodes

To ensure that the non-conductive coatings do not interfere with the electrophysiology recording, a set of functional electrodes was used to examine the effects of TNP+L1 coatings on the electrical property and recording capability over time (Figure 3). Impedance measurements were taken prior to surface modification (pristine) and all subsequent impedance modulus values were scaled to the pristine impedance. Following modification there was a slight increase in the impedances for the TNP and TNP+L1 electrodes, while the smooth L1 electrodes decreased slightly in impedance (Figure 3A). Impedances on all electrodes increased after implantation, but the increase in impedance was significantly

lower for the TNP+L1 modified electrode at two, three, and four weeks (Figure 3A). TNP+L1 single unit yield (% of channels that were able to record at least 1 single unit) was greatest at all time points and was significantly higher than all conditions when compared across timepoints (Figure 3B, $p<0.001$). The TNP+L1 coating did not appear to affect the SNR (Figure 3C), however, the TNP+L1 coating did produce a significant decrease in the recording noise at three and four weeks (Figure 3D,E).

2.5 Post-Mortem Histology

Neural nuclei were stained with NeuN (Figure 4A,D), and cell counts were quantified and normalized to control images (Figure 4B,E). Quantifying cell counts immediately adjacent to the electrode at 1-week post implantation revealed that control electrodes had significantly lower cell counts within the 100μm zone of implants than any other condition, while L1 and TNP+L1 electrodes showed the highest cell density. All electrodes exhibited a decrease in cell counts in the vicinity of the electrode compared to undisturbed regions of the brain, with relative cell counts approaching control tissues after 150μm from the implant surface (Figure 4C). The observed decrease in neurons adjacent to the electrode was no longer universally present after four weeks. At four weeks, neuron density was greatest adjacent to TNP+L1 electrodes, significantly higher than any other condition (Figure 4E). This result is even more interesting due to the neural cell density being greater than the control brain regions.

NF-200 staining was performed to examine the axonal growth after implantation (Figure 5A,D). At 1-week post implantation, a significant increase in NF-200 staining was observed for both nanoparticle-modified conditions within the 100μm zone (Figure 5B). By contrast at 4-weeks, the most intense staining was adjacent to the TNP+L1 electrode. The NF-200 intensity in the 100μm region adjacent to the TNP+L1 electrode was significantly higher than the region adjacent to the control electrode as well as the baseline value calculated from the control images. NF-200 intensity was also elevated near L1 modified electrodes, with the mean intensity higher than control images (intensity > 1) but not significantly different than the tissue proximal to the control electrode (Figure 5E). Regardless of experimental condition or timepoint, relative NF-200 staining intensity returned to baseline prior to the 225μm measurement (Figure 5C,F).

Host microglia were stained with Iba-1 (Figure 6A,D). At the 1-week timepoint, Iba-1 expression appeared to trend upwards after nanoparticle modification, however these results were not deemed significant ($p>0.05$, one-way ANOVA) (Figure 6B). After one week, the staining intensity verses distance was similar for all test conditions, with a peak staining intensity adjacent to the electrode followed by a decrease to baseline values after 100–150μm from the implant (Figure 6C). After four weeks, this trend was no longer apparent. The TNP modification produced the greatest increase in Iba-1 staining, while the TNP+L1 modification eliminated microglial encapsulation after 4 weeks (Figure 6E). Smooth conditions were nestled between the TNP modified conditions, with L1 modified probes exhibiting lower Iba-1 expression than smooth controls. The TNP intensity verses distance shows an interesting peak at 50μm from the implant (Fig 6F). The peak was attributed to low sample sizes for the 25μm bin due to tissue loss during brain removal.

Astrocytic activation was visualized by staining for GFAP (Figure 7A,D). At 1-week, GFAP staining was significantly higher in the control group than any of the experimental conditions (Figure 7B). The intensity verses distance graphs demonstrate the expected trend, with the highest GFAP staining being closest to the electrode and decreasing towards baseline. At 4-weeks post implantation, the L1 and TNP+L1 groups had significantly lower GFAP expression adjacent to the electrode compared to the control electrodes (Figure 7E).

The observed increase in neurons adjacent to the TNP+L1 electrode prompted investigation into the origin of these cells. Nestin (green) and DCX (red) stains were performed on the one and four week tissues (Figure 8A,D). At 1-week, an increase in nestin positive cells was observed for the TNP+L1 and TNP electrodes relative to the control (Figure 8B). Similarly, an increase in DCX positive cells was observed for all conditions relative to control at 1-week with TNP+L1 having the highest number of DCX positive cells (Figure 8C). The nestin and DCX staining dropped dramatically at four weeks. At the later time point, only the L1 modified smooth probe produced significant differences in nestin and DCX positive cells relative to the other probes (Figure 8E,F).

2.6 Explant Analysis

Explanted electrodes were examined under SEM to confirm the stability of the nanoparticle deposition *in vivo* (Figure 9). Regions adjacent to the skull were less tissue-encapsulated, and the particle modification was clearly visible (Figure 9A). Distal regions of the electrode were well coated with biological materials, and nanoparticles were not able to be directly observed by SEM. However, deformations in the biological tissue (diameter 147nm ± 17nm, mean ± SD) coincided well with the dimensions of the nanoparticles bound to the probe adjacent to the skull (159.2 ±15.6), suggesting their presence below the biological layer (Figure 9B,D). The biological encapsulation was also present on electrodes without TNP modifications, but the lack of underlying textural modification produced a smooth coating (Figure 9C).

3. Discussion

In this work, we examined the potential for the combination of bioactive molecules immobilization and modification of surface topography for a more stable electrode-tissue interface. We used nanoparticles to elevate the roughness of the surface. This modification increased the amount of bound protein and increased the biological lifetime of proteins.

Silica nanoparticles are an ideal candidate for surface topographical modification. A thiol modified silica nanoparticle was synthesized such that the particles would be covalently linked to GMBS modified substrates of either silica or silicon. The methods detailed here allow for precise tailoring of the chemical and morphological properties of silicon surfaces. The binding mechanism can be altered by changing the base silane, the crosslinking agent, or even the functionalization of the nanoparticles. The surface chemistry of the fully modified substrate is directly related to the surface chemistry of the silica nanoparticles. Exchanging the silane used during nanoparticle synthesis may allow for alkene, alkyne, amine, amide, epoxide, sulfonate, and many other surface functional groups. The topography may be readily tailored by changing the size of the nanoparticles, their concentration, or

changing the amount of interaction between particles to increase or reduce stacking. Unlike etching or focused ion beam milling, TNP modification can change the topography with minimal damage to the underlying substrate, which would otherwise be a concern when working with costly neural electrodes or other medical devices. Finally, the nanoparticle binding is stable both *in vitro* and *in vivo*, making the surface modification ideal for biologically interfacing devices.

We have previously reported the immobilization of proteins and other bioactive molecules to TNP modified surfaces.[27] The primary finding in that study was that significantly more L1 bind to the roughened surface and this higher surface density translated to higher bioactivity manifested as longer neurite extension. In this study, we specifically examined the longevity of the protein coating by soaking samples at physiological conditions for extended periods of time to simulate the *in vivo* application, and examined the amount of bound proteins and their bioactivity. First, we observed an increase in the amount of protein bound to the TNP modified substrates. In addition, TNP modified substrates maintained their bound protein better under physiological conditions. The increase in bound protein translated to enhanced bioactivity of the substrates.

The increase in stability may be attributed to a few factors, including an increase in the amount of bound protein,[27] a decrease in deterioration of the protein,[50] complementary interactions of topography and protein modifications, and stronger binding of the protein to the TNP substrate compared to the smooth substrate. TNP surface modification has previously demonstrated to increase the amount of protein bound to the surface by increasing the available binding locations. If the surface bound concentration of L1 is greater than the concentration detectable by neurons, then loss of a small portion of the bound L1 should not affect the neurite outgrowth. Conversely, the L1 binding may be below the highest effective level but capable of maintaining its bioactivity for longer when bound to the TNP substrate. Binding of the L1 to multiple locations may increase the bioactive lifetime. L1 bound to a single location on the surface would be removed by breaking any chemical bond in the protein backbone or crosslinker, making the binding mechanism precarious. L1 scaffolded to the TNP modified surface may have a greater number of binding sites with the surface and be far less likely to de-couple during the incubation period.

In addition to maintaining the bioactivity of the L1, the possibility of a cooperative effect between the protein and topographical modifications should not be ignored. This idea is supported by the observation that the TNP modification was sufficient to increase neurite outgrowth compared to smooth chemistry-matched samples, and that the L1 maintained a small degree of activity on smooth surfaces after 28 days. The synergistic effect of the TNP+L1 coating may be sufficient to maintain the neurite outgrowth even as the L1 itself decreases in activity.

Rough substrates have previously been shown to enhance neurite outgrowth and attachment, [37, 39, 51, 52] with the maximum outgrowth seen for surface roughness between 20nm and 70nm.[37] These findings are further supported by this work, with the calculated roughness of the TNP modified substrates (78.6nm ± 0.2nm) just above the upper limit. The

discrepancy may be explained by the mathematical representation of roughness. Roughness calculations are imperfect representations of surface topography, most often relying on deviations from the mean height of the sample and not the size/shape of the surface features. The aforementioned ideal roughness was measured on etched silicon, producing a more jagged surface topography than TNP immobilization. The smoother TNP coating may have a different ideal roughness, and further examination of neurite outgrowth on nanoparticle modified surfaces may provide invaluable information regarding the interplay of roughness, particle size, and neurite extension.

We observed that the NPs not only cover the silicon oxide portion of the neural probe, but also the electrode sites. One valid concern is whether the non-conductive NP coating will block signal transduction and consequently compromising the recording capability. The impedance of the electrodes was increased by <150kΩ after the TNP and TNP+L1 coatings, a change which is unlikely to affect recording performance. The TNP+L1 electrodes had the lowest *in vivo* impedances at three and four weeks, negating any initial impedance increases due to modification. Interestingly, a slight decrease in the impedance of the L1 modified electrodes was observed, which could be attributed to the additional cleaning of the electrode site during surface modification. In addition, bound proteins can affect the charge exchange at the electrode/electrolyte interface,[53] and the slightly negatively charged L1 may also have contributed to the observed impedance change. The implanted TNP+L1 electrodes maintained the lowest *in vivo* impedances of the tested conditions, potentially indicating that the modification could minimize glial encapsulation at the electrode site. Additionally, the TNP+L1 modification increased the single unit yield of the modified electrodes compared to the other conditions, further confirming the functionality of the electrode was not compromised by the non-conductive coating. The increased recording yield could be a result of higher neuron density at the vicinity of the probe with the TNP-L1 showing the highest yield and highest neuron density among all groups. Noise was also lowered by the TNP+L1 modification due to the decreased impedances. Johnson noise was calculated by the equation:

$$V_{noise} = \sqrt{4k_B RT\Delta f}$$

Where k_B is the Boltzman Constant (1.38×10^{-23} J K^{-1}), R is the real impedance, T is temperature in Kelvin, and Δf is the sampling frequency. The calculated values of V_{noise} for the TNP+L1 and TNP electrodes at week four are 9.57μV and 14.72μV, respectively. The measured noise values of 11.28μV and 15.81μV align well with the calculated values. With lower noise, additional low amplitude units may be captured which can lead to higher yield but lower average peak to peak amplitude.

Neural electrodes rely on the proximity of the electrode sites and neural somas to be within 140μm[54] and closer distances are heavily preferred. The neuron cell density at the vicinity of the implant was higher for the L1 modified electrodes compared to control and TNP modified groups, but overall cell density was dramatically lower than control tissues at the 1-week time point. The general decrease in neuron cell density is likely due to insertion injury and the strong acute response to the implant. Neuron density adjacent to the electrode

was recovered at four weeks and was even elevated above control tissue for the L1 and TNP+L1 modified conditions. Such increase in neuronal density is likely to contribute to the elevated single unit yield. The increased presence of neuron somas adjacent to the electrode could be due to a number of reasons: 1) tissue compression after electrode insertion along with the lack of cellular death around the L1 coated probes due to the anti-inflammatory and neuroadhesive effect L1 and 2) migration of neurons to the site of injury and neurogenesis.

Nestin and DCX staining was performed to examine the origin of the neurons around the implanted electrodes. Nestin is expressed in neural stem and progenitor cells and endothelial cells during angiogenesis.[55] The increase in nestin staining at 1-week post implantation indicates that tissue healing has commenced, and new cells and vessels are present adjacent to the probe. This response appears to be most prominent adjacent to the TNP+L1 electrode. This expression decreases at the four-week timepoint for all conditions, possibly indicating that the new tissues around the electrode have begun maturing. DCX is used as a marker of immature neurons[56] and increases in DCX staining may indicate that immature neurons are present adjacent to the electrode after injury. DCX positive cells have been observed following implantation of mesh electrodes, potentially due to migration of neurons to the site of implantation.[57] At 1-week post implantation, a significant increase in the DCX positive cells was observed in both L1 and L1+TNP groups, further suggesting that neurons in the area may have formed recently. Similar to the nestin staining, the number of DCX positive cells decreased at the 4-week timepoint as the cells mature. The increase in nestin and DCX staining for the L1, TNP, and TNP+L1 is a promising indication of the beneficial effects of both topographical and bioactive modifications. The positive nestin and DCX staining are very promising, but a more intensive characterization is required to confirm the origin and age of the neurons and whether these cells can contribute to the recording yield.

The axonal densities were similar between all groups at 1-week post implantation, however there was a small but significant increase in the NF-200 staining directly adjacent to the TNP and TNP+L1 modified electrodes relative to the control and L1 groups. At 4 weeks, the two L1 modified conditions exhibited significantly increased NF-200 staining relative to control and TNP groups. Unlike somas, regeneration is more commonly observed in axons. The increase in NF-200 staining is attributed to a combination of axonal regeneration, adhesion to the L1-modified electrode, and tissue compression/remodeling after insertion. L1 is a potent promoter of neurite extension in vitro and axonal regeneration *in vivo*.[30, 31, 58, 59] The axonal promoting effect of L1 coating on neural probe has been previously reported by our group.[11, 33, 60] The result here is consistent with the previous finding.

Staining microglia and astrocytes allowed for the examination of non-neural cell responses to the implanted foreign body. Contrary to expectations, at the 1-week time point there was an elevated, yet not significant, iba-1 expression adjacent to the TNP+L1 electrodes. This result reversed itself at the 4-week timepoint, with the TNP+L1 modified electrodes performing significantly better than all other treatments. Previous experiments have concluded that L1 minimized microglial activation after contact, such that the cells still respond to the implant but after examining the surface do not continue forward to traditional encapsulation.[35] Here, we see that at the early time point the microglia are still in the process of examining the implant. At 4-weeks, the TNP+L1 electrodes exhibited no

microglial encapsulation. The complete lack of microglial activation for TNP+L1 electrodes is attributed to the increased stability of the L1 coating, remaining active throughout the initial inflammation and allowing for the formation of a healthier electrode-tissue interface. TNP modification itself did not lead to decreased immune response, instead increasing microglial encapsulation at 4-weeks. The increase in glial response may be caused by the increased binding of blood proteins to the TNP surface, or detachment of a small number of particles which then caused an additional immune response. Rosengren et al. found that encapsulation of smooth electrodes increased between 6 and 12 weeks, while encapsulation of porous surfaces decreased or remained constant.[61] Therefore, it remains to be important to investigate how inflammatory responses evolve over longer implantation time for the TNP surface.

Increased expression of GFAP in astrocytes is often observed after brain injury as the tissue forms a scar around the damaged area.[62] At the one-week timepoint, differences in astrocytic encapsulation were observable between the control electrodes and all three experimental conditions. Astrocytic encapsulation occurs after microglial,[10] and was expected to be more predominant at the 4-week time point. At this time point, L1 and TNP+L1 electrodes elicited significantly lower encapsulation than the control electrodes. Notably, the TNP modification alone was not able to affect the astrocytic encapsulation at four weeks. While previous work has demonstrated that topographical modifications are sufficient to limit astrocytic spreading *in vitro*, the presence of L1 appears to be required to translate these findings *in vivo*.[27]

Finally, it is necessary to confirm the attachment of the nanoparticles after explantation. The adhesion of the particle to the electrode must be maintained throughout the study for the L1 coating to maintain its function. Furthermore, unbound nanoparticles may increase inflammation as phagocytic cells try to remove them from the implant vicinity. The binding of the nanoparticles to the surface was studied with SEM after explanting the electrodes, verifying that the TNP and TNP+L1 modifications are stable throughout the 4-week experiment. SEM is not capable of confirming that no nanoparticles detached *in vivo*, and removal of a small percentage of the nanoparticles may have occurred without being detected. While not performed in this study, more direct measurements of the nanoparticle layer (surface area and roughness) before implantation and after explantation would provide a more quantitative assessment of nanoparticle layer stability. However, the bulk of the coating remained intact after explantation and maintained its bioactivity throughout the time course of this study. Together with previous studies which have examined the adhesion of the nanoparticles and silicon substrates,[27] there is sufficient evidence to indicate the maintenance of nanoparticle adhesion for at least 4-weeks *in vivo*.

4. Conclusions

In this work we have explored the combined use of nano topographical and bioactive surface modifications for use on neural implants. *In vitro* we observed that the nanoparticle modification was successful at both increasing the bioactivity of the L1 surface modification, as well as maintaining that activity for up to four weeks at 37°C in PBS. *In vivo*, the L1+TNP modification outperformed both individual modifications

(TNP and L1 respectively) by demonstrating the highest single unit recording yield, highest number of neural somas adjacent to the electrode, and eliminated microglial reactions after four weeks. Elevated expression of DCX and nestin adjacent to the TNP+L1 electrode may indicate that neural stem/progenitor cells may have migrated to the electrode site after implantation and some of them underwent neuronal differentiation. Additionally, the nanoparticle modification was stable for the course of the experiment. Together, we have found that the combined nanoparticle and bioactive L1 surface modifications offer an opportune method of increasing chronic electrophysiologic recording performance by enhancing both the bioactivity and lifetime of protein surface modifications, without risk of damage to the device.

5. Experimental Section

All reagents were purchased through Acros Organics (Fair Lawn, NJ) and used as purchased unless otherwise stated. Tetraethyl orthosilicate (TEOS) was purchased from Millipore-Sigma (Burlington, MA). Silicon wafer was purchased through University Wafer (Boston, MA), glass coverslips through Electron Microscopy Sciences (Hatfield, PA), and silicon electrodes were supplied by NeuroNexus (Ann Arbor, MI). Functional electrodes were model A1×16–3mm-100–703, with 16 electrode sites, a total length of 3mm, electrode diameter of 30μm, and 1kHz impedances between 200kΩ and 400kΩ, and dummy electrodes were matched to this geometry but without the functional connector attached. Fluorescence imaging was performed on a Leica DMI4000b. Brain slicing was performed with a Leica CM 1950 cryostat. Confocal images were taken by Olympus Fluoview 1000. Scanning electron microscopy (SEM) images were taken by JSM6335. Particle sizes were measured with ImageJ. Water contact angle (WCA) measurements were performed with AST Products VCA Optima. Ellipsometry measurements were performed on J. A. Woollam α-SE, data were analyzed with a Cauchy model, assigning a refractive index of 1.45.

Nanoparticle Synthesis:

Thiol modified nanoparticles were fabricated as previously described.[63] In brief, a solution of water (36mL), ethanol (5mL), and triethanolamine (6.18mL) was heated to 60°C. Under vigorous stirring, TEOS (3mL) was added dropwise. The reaction was allowed to proceed for 5 minutes, at which point mercaptopropyl trimethoxysilane (MTS, 1mL) was added. The reaction continued under stirring for 1 hour, then additional MTS (250μl) was added and the reaction continued for 1 additional hour. Particles were collected from suspension via centrifuge and washed with ethanol and water.

Particle immobilization:

Substrates (silicon wafer, glass coverslips, or silicon probes) were washed with acetone and isopropanol, followed by activation under oxygen plasma for 5 minutes. Functional electrodes were grasped with a stereotaxic frame by the tab, while dummy probes were secured to a plastic tab which was secured to a stereotaxic frame. The activated substrates were immersed in aminopropyl triethoxysilane (APTES) or MTS at 2.5v/v% in ethanol for 1 hour then washed thoroughly with ethanol followed by water. MTS coated substrates were removed at this point to serve as chemistry matched smooth control compared to TNP

electrodes. APTES modified substrates were immersed in GMBS solution (2mg mL^{-1} in phosphate-buffered saline (PBS)) for 30 minutes, then washed with water. A nanoparticle suspension was made by sonicating TNP (10mg) in 0.1x PBS (10mL), diluted with double DI-water. APTES-GMBS modified substrates were immersed in the nanoparticle suspension for 1 hour at 37°C, with constant agitation provided by either an orbital shaker (for glass/silicon) or a small stir bar (probes).

L1 Isolation:

L1 was isolated from rat brain tissues as previously described.[30] In brief, brains were isolated from p16–20 rat pups and the membrane was isolated and solubilized in CHAPs buffer. The solubilized membrane was then passed through an antibody affinity column and L1 protein was eluted by the addition of diethylamine solution at pH 11.5. L1 samples were collected, combined, and stored at −80°C. Before use, L1 solutions were thawed and dialyzed to remove diethylamine.

Protein Immobilization:

Protein immobilization was performed on either smooth MTS modified substrates or TNP modified substrates. Substrates were re-immersed in GMBS solution (2mg mL^{-1}), followed by washing and submerging of the substrates in L1 solution (50μg mL^{-1}) for 1 hour at 37°C. L1 was immobilized to 18mm glass coverslip pre-modified with TNP or MTS and the slides were placed into 12 well plates. Half of the modified coverslips were dried thoroughly, and the remaining submerged in PBS (2mL). The plate was then incubated for one or four weeks, after which all samples were washed with DI water. L1 was digested off the samples with 6N HCl for 24H at 80C in sealed containers. The peptide concentration was measured by UV-absorbance of the sample at 280nm.

In Vitro Experiments:

To examine the long-term bioactivity of L1 after immobilization, 10 groups of coverslips were created, split between TNP modified coverslips and smooth MTS modified coverslips, with at least 5 samples per condition and 3 experimental repeats. 4 weeks before cell culture, 1 group of smooth and TNP modified glass was immersed in GMBS solution followed by L1 immobilization as described above. The samples were then washed and stored in PBS in a cell culture incubator. This procedure was repeated at 7 and 3 days before cell culture, as well as the day of culture.

Primary neurons were isolated from rat E18 fetuses. The mother rat was euthanized under CO_2 followed by cervical dislocation, at which point the pups were removed and placed in ice-cold Hanks balanced salt solution (HBSS). Individually, a pup was isolated, decapitated, and the brain removed. The cortex was isolated and submerged in .15% trypsin solution for 15 minutes at 37°C. The brain was washed with HBSS and dissociated via trituration. The supernatant was collected and cells concentrated via centrifuge. Cells were resuspended in Neurobasal media, supplemented with B27, GlutaMAX, and Pen/Strep, then counted and plated at a density of 25,000 cells cm^{-2}. Cells were grown for 36 hours, then fixed with 4% paraformaldehyde (PFA). Fixed cells were permeabilized with 0.2% Triton-X in PBS, followed by immuno-staining for b(III)-tubulin and DAPI.

Surgery and Implantation:

All animal work was performed under the guidelines of the University of Pittsburgh Institutional Animal Care and Use Committee (IACUC). A mouse model was chosen to examine the effects of topographical and bioactive modification *in vivo*, scheme 2. Four experimental conditions were chosen to elucidate the individual and combinatorial effects of topography and proteins: control (MTS modified), L1 (MTS modified with immobilized L1), TNP (TNP modified), and TNP+L1 (TNP modified with immobilized L1). The control condition is included to assess the baseline histological responses to the implants. For acute (1 week) and chronic (4 week) histology, mice (C57-BL6) were anesthetized under isoflurane gas (1.5%) and the surgical area sterilized with iodine solution and 70% ethanol. The scalp was removed, and 4 probe holes spaced 2mm apart in a square configuration were made in the left skull, between lambda and bregma. An additional hole was made for an anchor screw to be attached. Into each animal, 1 dummy probe of each condition was implanted 2mm deep with a stereotaxic manipulator, with the order randomized. Probe holes were then sealed with silicone-epoxy. A skull cap was then formed with UV-curable dental cement, and the wound was closed by suturing around the skull cap. Four animals were implanted for each time-point, each with four electrodes, one of each experimental condition.

Chronic Electrophysiology:

For electrophysiology assessment, functional electrodes were implanted in the same manner as above but were limited to one electrode per animal and electrodes were inserted into the left visual cortex. Three bone screws were placed into the skull, two anterior to the electrode, and 1 on the adjacent hemisphere to stabilize the headcap. The visual cortex was located by measuring 1mm anterior to the lambda, and 1.5mm from the midline. A small hole was drilled and the electrode was inserted with a stereotaxic manipulator such that all electrode sites were in the cortex. The hole was then sealed with silicone epoxy and the omnetic connector was stabilized by a headcap created from UV-curable dental acrylic. Chronic data was gathered from six animals per condition.

Impedance measurements and electrophysiological recordings were performed as previously described. [64] In brief, Impedance measurements were performed on an AutoLab potentiostat, sampled between 32kHz and 10Hz. Electrophysiological recordings were performed under 1% isoflurane anesthesia. The resulting data was sampled at 24,414Hz (RX7, Tucker-Davis Technologies) prior to being analyzed under a custom MatLab script. The data stream was filtered between 300 and 5000Hz for identification of single units. Single unit snippets (1.2ms) were isolated by threshold crossing events greater than 3.5 standard deviations of the noise, then manually sorted based on waveform and spike timing. Snippets were removed from the data prior to the calculation of the peak to peak noise.[65] Signal to noise ratio (SNR) was calculated as the mean peak to peak voltage of the greatest single unit waveform divided by two standard deviations of the noise.

Perfusion:

At the experimental end points, mice were deeply anesthetized with a ketamine/xylazine cocktail and perfused with 100mL PBS followed by 100 mL 4% PFA. The bottom of the

skull was then removed and the brains, still attached to the upper scull, were post fixed in 4% PFA for 4 hours. The brains were then removed from the skull, sucrose protected, frozen, and cryosectioned. The electrodes remained attached to the skull and were removed from the brain when the brain was separated from the upper skull. Brain slices were rehydrated and immunostained.

Immunostaining and Histology:

Brain slices were rehydrated with PBS then blocked with 10% goat serum, following which the brain slices were treated with 0.1% Triton-x for 45 minutes. Staining of the brains was performed in groups consisting of NeuN (Millipore mouse 1:250), NF200 (Abcam rabbit 1:500), Iba-1 (Millipore mouse 1:500), GFAP (DAKO rabbit 1:500), nestin (Millipore mouse 1:200), and DCX (Abcam rabbit 1:1000). A confocal microscope (Olympus flowview-1000) was used to take fluorescent images of each of the four implanted areas as well as the un-implanted contralateral tissue. All stained implant site images were quantified relative to control images of the contralateral hemisphere that did not receive implants. A subset of the data between 0 and 50μm from the implant surface was plotted in addition to the entire 225μm measured area in order to evaluate significance of stained groups immediately adjacent to the implant surface. The probes, which remained connected to the skull after removal of the brain, were then gathered by snapping the shank proximal to the skull. Finally, the probes were dehydrated with ethanol and hexamethyldisilazane for SEM imaging. Particle sizes were determined by measuring width in ImageJ, then scaled to nanometers.

Statistical Analysis:

All statistical comparisons were made with GraphPad Prism 8. Significance was defined as *$p < 0.05$, **$p<0.01$, ***$p<0.001$, and ****$p<0.0001$. When applicable, all data is displayed as mean ± standard error. WCA and roughness measurements were gathered from nine samples. Bound protein quantification was measured from three trials, each with three aged smooth and rough experimental samples and three control smooth and rough samples. Measured protein concentrations were then normalized to the control smooth condition. Comparisons between rough and smooth substrates were made using a two-sided student’s T-test with a Bonferroni correction, and comparisons across time were made with a one-way ANOVA followed by Tukey’s post-hoc. Neurite outgrowth quantifications were from 4 separate trials, each with 3 samples per condition. Multiple random images were taken per sample and averaged prior to additional processing. Statistical significance was determined with a two-way ANOVA and Tukey’s post hoc. Electrochemical measurements and electrophysiological recording performance were measured from six animals per condition and compared with two-way ANOVA and Tukey’s post hoc. The initial *in vitro* impedances were subtracted from the remaining measured impedances. Histology was gathered from four animals per time point. Differences were determined with a one-way ANOVA and Tukey’s post hock (Figures 4–7B,E and Figure 8B,C,E,F).

Acknowledgements

This work was funded by the following grants: NIH NINDS R01 1R01NS089688, R01NS062019, R21DA049592 and BRAIN R01NS110564 and U01NS113279. We thank the Center for Biological Imaging at the University of Pittsburgh for the confocal microscopy support.

References

[1]. Schwartz AB, Cui XT, Douglas JWeber, D.W. Moran, Brain-Controlled Interfaces: Movement Restoration with Neural Prosthetics, Neuron52(1) (2006) 205–220. [PubMed: 17015237]

[2]. Sussillo D, Stavisky SD, Kao JC, Ryu SI, Shenoy KV, Making brain–machine interfaces robust to future neural variability, Nature Communications7(1) (2016) 13749.

[3]. Collinger JL, Boninger ML, Bruns TM, Curley K, Wang W, Weber DJ, Functional priorities, assistive technology, and brain-computer interfaces after spinal cord injury, J Rehabil Res Dev50(2) (2013) 145–160. [PubMed: 23760996]

[4]. Wightman RM, Strope E, Plotsky PM, Adams RN, Monitoring of transmitter metabolites by voltammetry in cerebrospinal fluid following neural pathway stimulation, Nature262(5564) (1976) 145–146. [PubMed: 934333]

[5]. Yamada Y, Ueshima H, Methods of Electrophoretical Application of Estrogen to a Single Neuron of the Brain under *in vivo* and *in vitro* Conditions, Endocrinologia Japonica25(4) (1978) 397–401. [PubMed: 710374]

[6]. Castagnola E, Woeppel K, Golabchi A, McGuier M, Chodapaneedi N, Metro J, Taylor IM, Cui XT, Electrochemical detection of exogenously administered melatonin in the brain, Analyst145(7) (2020) 2612–2620. [PubMed: 32073100]

[7]. Taylor IM, Du Z, Bigelow ET, Eles JR, Horner AR, Catt KA, Weber SG, Jamieson BG, Cui XT, Aptamer-functionalized neural recording electrodes for the direct measurement of cocaine in vivo, Journal of Materials Chemistry B5(13) (2017) 2445–2458. [PubMed: 28729901]

[8]. Taylor IM, Robbins EM, Catt KA, Cody PA, Happe CL, Cui XT, Enhanced dopamine detection sensitivity by PEDOT/graphene oxide coating on in vivo carbon fiber electrodes, Biosensors and Bioelectronics89 (2017) 400–410. [PubMed: 27268013]

[9]. Hu Y, Mitchell KM, Albahadily FN, Michaelis EK, Wilson GS, Direct measurement of glutamate release in the brain using a dual enzyme-based electrochemical sensor, Brain Research659(1) (1994) 117–125. [PubMed: 7820652]

[10]. Polikov VS, Tresco PA, Reichert WM, Response of brain tissue to chronically implanted neural electrodes, Journal of Neuroscience Methods148(1) (2005) 1–18. [PubMed: 16198003]

[11]. Azemi E, Lagenaur C, Cui XT, The Surface Immobilization of the Neural Adhesion Molecule L1 on Neural Probes and its Effect on Neuronal Density and Gliosis at the Probe/Tissue Interface, Biomaterials32(3) (2011) 681–692. [PubMed: 20933270]

[12]. Kozai TDY, Langhals NB, Patel PR, Deng X, Zhang H, Smith KL, Lahann J, Kotov NA, Kipke DR, Ultrasmall implantable composite microelectrodes with bioactive surfaces for chronic neural interfaces, Nature Materials11 (2012) 1065. [PubMed: 23142839]

[13]. Takeuchi S, Ziegler D, Yoshida Y, Mabuchi K, Suzuki T, Parylene flexible neural probes integrated with microfluidic channels, Lab on a Chip5(5) (2005) 519–523. [PubMed: 15856088]

[14]. Kuo JTW, Kim BJ, Hara SA, Lee CD, Gutierrez CA, Hoang TQ, Meng E, Novel flexible Parylene neural probe with 3D sheath structure for enhancing tissue integration, Lab on a Chip13(4) (2013) 554–561. [PubMed: 23160191]

[15]. Gao K, Li G, Liao L, Cheng J, Zhao J, Xu Y, Fabrication of flexible microelectrode arrays integrated with microfluidic channels for stable neural interfaces, Sensors and Actuators A: Physical197 (2013) 9–14.

[16]. Du ZJ, Kolarcik CL, Kozai TDY, Luebben SD, Sapp SA, Zheng XS, Nabity JA, Cui XT, Ultrasoft microwire neural electrodes improve chronic tissue integration, Acta Biomaterialia53 (2017) 46–58. [PubMed: 28185910]

[17]. Golabchi A, Wu B, Li X, Carlisle DL, Kozai TDY, Friedlander RM, Cui XT, Melatonin improves quality and longevity of chronic neural recording, Biomaterials180 (2018) 225–239. [PubMed: 30053658]

[18]. Zhong Y, Bellamkonda RV, Dexamethasone-coated neural probes elicit attenuated inflammatory response and neuronal loss compared to uncoated neural probes, Brain Research1148 (2007) 15–27. [PubMed: 17376408]

[19]. Potter KA, Buck AC, Self WK, Callanan ME, Sunil S, Capadona JR, The effect of resveratrol on neurodegeneration and blood brain barrier stability surrounding intracortical microelectrodes, Biomaterials34(29) (2013) 7001–7015. [PubMed: 23791503]

[20]. Potter-Baker KA, Nguyen JK, Kovach KM, Gitomer MM, Srail TW, Stewart WG, Skousen JL, Capadona JR, Development of superoxide dismutase mimetic surfaces to reduce accumulation of reactive oxygen species for neural interfacing applications, Journal of Materials Chemistry B2(16) (2014) 2248–2258. [PubMed: 25132966]

[21]. Zheng XS, Snyder NR, Woeppel K, Barengo JH, Li X, Eles J, Kolarcik CL, Cui XT, A superoxide scavenging coating for improving tissue response to neural implants, Acta Biomaterialia99 (2019) 72–83. [PubMed: 31446048]

[22]. Wei H, George CM, Ravi VB, Nanoscale laminin coating modulates cortical scarring response around implanted silicon microelectrode arrays, Journal of Neural Engineering3(4) (2006) 316. [PubMed: 17124336]

[23]. Stauffer WR, Cui XT, Polypyrrole doped with 2 peptide sequences from laminin, Biomaterials27(11) (2006) 2405–2413. [PubMed: 16343612]

[24]. Bhagwat N, Murray RE, Shah SI, Kiick KL, Martin DC, Biofunctionalization of PEDOT films with laminin-derived peptides, Acta Biomaterialia41 (2016) 235–246. [PubMed: 27181880]

[25]. Cui X, Lee VA, Raphael Y, Wiler JA, Hetke JF, Anderson DJ and Martin DC, Surface modification of neural recording electrodes with conducting polymer/biomolecule blends, Journal of biomedical materials research 56 (2001) 261–272. [PubMed: 11340598]

[26]. Sikder KU, Tong W, Pingle H, Kingshott P, Needham K, Shivdasani MN, Fallon JB, Seligman P, Ibbotson MR, Prawer S, Garrett DJ, Laminin coated diamond electrodes for neural stimulation, Materials Science and Engineering: C (2020) 111454.

[27]. Woeppel KM, Zheng XS, Cui XT, Enhancing surface immobilization of bioactive molecules via a silica nanoparticle based coating, Journal of Materials Chemistry B6(19) (2018) 3058–3067. [PubMed: 30464839]

[28]. Azemi E, Stauffer WR, Gostock MS, Lagenaur CF, Cui XT, Surface immobilization of neural adhesion molecule L1 for improving the biocompatibility of chronic neural probes: In vitro characterization, Acta Biomaterialia4(5) (2008) 1208–1217. [PubMed: 18420473]

[29]. Kolarcik CL, Bourbeau D, Azemi E, Rost E, Zhang L, Lagenaur CF, Weber DJ, Cui XT, In vivo effects of L1 coating on inflammation and neuronal health at the electrode–tissue interface in rat spinal cord and dorsal root ganglion, Acta Biomaterialia8(10) (2012) 3561–3575. [PubMed: 22750248]

[30]. Lagenaur C, Lemmon V, An L1-like molecule, the 8D9 antigen, is a potent substrate for neurite extension, Proceedings of the National Academy of Sciences of the United States of America84(21) (1987) 7753–7757. [PubMed: 3478724]

[31]. Xu G, Nie D.-y., Wang W.-z., Zhang P.-h., Shen J, Ang B.-t., Liu G.-h., Luo X.-g., Chen N.-l., Xiao Z.-c., Optic nerve regeneration in polyglycolic acid–chitosan conduits coated with recombinant L1-Fc, NeuroReport15(14) (2004).

[32]. Martini R, Expression and functional roles of neural cell surface molecules and extracellular matrix components during development and regeneration of peripheral nerves, Journal of Neurocytology23(1) (1994) 1–28. [PubMed: 8176415]

[33]. Golabchi A, Woeppel KM, Li X, Lagenaur CF, Cui XT, Neuroadhesive protein coating improves the chronic performance of neuroelectronics in mouse brain, Biosensors and Bioelectronics155 (2020) 112096. [PubMed: 32090868]

[34]. Cody PA, Eles JR, Lagenaur CF, Kozai TDY, Cui XT, Unique electrophysiological and impedance signatures between encapsulation types: An analysis of biological Utah array failure

and benefit of a biomimetic coating in a rat model, Biomaterials161 (2018) 117–128. [PubMed: 29421549]

[35]. Eles JR, Vazquez AL, Snyder NR, Lagenaur C, Murphy MC, Kozai TDY, Cui XT, Neuroadhesive L1 coating attenuates acute microglial attachment to neural electrodes as revealed by live two-photon microscopy, Biomaterials113 (2017) 279–292. [PubMed: 27837661]

[36]. Wu Z-Z, Zhao Y, Kisaalita WS, Interfacing SH-SY5Y human neuroblastoma cells with SU-8 microstructures, Colloids and Surfaces B: Biointerfaces52(1) (2006) 14–21. [PubMed: 16837176]

[37]. Fan YW, Cui FZ, Hou SP, Xu QY, Chen LN, Lee IS, Culture of neural cells on silicon wafers with nano-scale surface topograph, Journal of Neuroscience Methods120(1) (2002) 17–23. [PubMed: 12351203]

[38]. Khan SP, Auner GG, Newaz GM, Influence of nanoscale surface roughness on neural cell attachment on silicon, Nanomedicine: Nanotechnology, Biology and Medicine1(2) (2005) 125–129.

[39]. Kim M-H, Park M, Kang K, Choi IS, Neurons on nanometric topographies: insights into neuronal behaviors in vitro, Biomaterials Science2(2) (2014) 148–155. [PubMed: 32481875]

[40]. Amin H, Dipalo M, De Angelis F, Berdondini L, Biofunctionalized 3D Nanopillar Arrays Fostering Cell Guidance and Promoting Synapse Stability and Neuronal Activity in Networks, ACS Applied Materials & Interfaces10(17) (2018) 15207–15215. [PubMed: 29620843]

[41]. Brüggemann D, Michael KE, Wolfrum B, Offenhäusser A, Adhesion and survival of electrogenic cells on gold nanopillar array electrodes, International Journal of Nano and Biomaterials4(2) (2012) 108–127.

[42]. Xie C, Lin Z, Hanson L, Cui Y, Cui B, Intracellular recording of action potentials by nanopillar electroporation, Nat Nanotechnol7(3) (2012) 185–190. [PubMed: 22327876]

[43]. Mahairaki V, Lim SH, Christopherson GT, Xu L, Nasonkin I, Yu C, Mao H-Q, Koliatsos VE, Nanofiber Matrices Promote the Neuronal Differentiation of Human Embryonic Stem Cell-Derived Neural Precursors In Vitro, Tissue Engineering Part A17(5–6) (2010) 855–863. [PubMed: 20973749]

[44]. Gertz CC, Leach MK, Birrell LK, Martin DC, Feldman EL, Corey JM, Accelerated neuritogenesis and maturation of primary spinal motor neurons in response to nanofibers, Developmental Neurobiology70(8) (2010) 589–603. [PubMed: 20213755]

[45]. Chapman CAR, Chen H, Stamou M, Biener J, Biener MM, Lein PJ, Seker E, Nanoporous Gold as a Neural Interface Coating: Effects of Topography, Surface Chemistry, and Feature Size, ACS Applied Materials & Interfaces7(13) (2015) 7093–7100. [PubMed: 25706691]

[46]. Brüggemann D, Nanoporous Aluminium Oxide Membranes as Cell Interfaces, Journal of Nanomaterials2013 (2013) 460870.

[47]. Posati T, Pistone A, Saracino E, Formaggio F, Mola MG, Troni E, Sagnella A, Nocchetti M, Barbalinardo M, Valle F, Bonetti S, Caprini M, Nicchia GP, Zamboni R, Muccini M, Benfenati V, A Nanoscale Interface Promoting Molecular and Functional Differentiation of Neural Cells, Scientific Reports6(1) (2016) 31226. [PubMed: 27503424]

[48]. Ereifej ES, Matthew HW, Newaz G, Mukhopadhyay A, Auner G, Salakhutdinov I, VandeVord PJ, Nanopatterning effects on astrocyte reactivity, Journal of Biomedical Materials Research Part A101A(6) (2013) 1743–1757.

[49]. S. EE, S. SC, M. MS, Keying C, He F, R. CJ, The Neuroinflammatory Response to Nanopatterning Parallel Grooves into the Surface Structure of Intracortical Microelectrodes, Advanced Functional Materials28(12) (2018) 1704420.

[50]. Yu X, Biedrzycki Adam H, Khalil Andrew S, Hess D, Umhoefer Jennifer M, Markel Mark D, Murphy William L, Nanostructured Mineral Coatings Stabilize Proteins for Therapeutic Delivery, Advanced Materials29(33) (2017) 1701255.

[51]. Ariano P, Budnyk O, Dalmazzo S, Lovisolo D, Manfredotti C, Rivolo P, Vittone E, On diamond surface properties and interactions with neurons, The European Physical Journal E30(2) (2009) 149.

[52]. Raffa V, Pensabene V, Menciassi A, Dario P, Design criteria of neuron/electrode interface. The focused ion beam technology as an analytical method to investigate the effect of electrode surface

morphology on neurocompatibility, Biomedical Microdevices9(3) (2007) 371–383. [PubMed: 17235683]

[53]. Liao W, Randall BA, Alba NA, Cui XT, Conducting polymer-based impedimetric aptamer biosensor for in situ detection, Analytical and Bioanalytical Chemistry, 392 (2008) 861–864. [PubMed: 18784918]

[54]. Buzsáki G, Large-scale recording of neuronal ensembles, Nature Neuroscience7(5) (2004) 446–451. [PubMed: 15114356]

[55]. Suzuki S, Namiki J, Shibata S, Mastuzaki Y, Okano H, The neural stem/progenitor cell marker nestin is expressed in proliferative endothelial cells, but not in mature vasculature, J Histochem Cytochem58(8) (2010) 721–730. [PubMed: 20421592]

[56]. Rao MS, Shetty AK, Efficacy of doublecortin as a marker to analyse the absolute number anddendritic growth of newly generated neurons in the adult dentate gyrus, European Journal of Neuroscience19(2) (2004) 234–246.

[57]. Yang X, Zhou T, Zwang TJ, Hong G, Zhao Y, Viveros RD, Fu T-M, Gao T, Lieber CM, Bioinspired neuron-like electronics, Nature Materials18(5) (2019) 510–517. [PubMed: 30804509]

[58]. Hortsch M, The L1 family of neural cell adhesion molecules: old proteins performing new tricks, Neuron17 (1996).

[59]. Kamiguchi H, Lemmon V, Neural cell adhesion molecule L1: signaling pathways and growth cone motility, J Neurosci Res49 (1997).

[60]. Yang ML, Li Y, Chilukuri K, Boulos MI, Kappes JC, Galileo DS: L1 stimulation of human glioma cell motility correlates with FAK activation. Submitted for publication.

[61]. Rosengren A, Wallman L, Danielsen N, Laurell T, Bjursten LM, Tissue reactions evoked by porous and plane surfaces made out of silicon and titanium, IEEE Transactions on Biomedical Engineering49(4) (2002) 392–399. [PubMed: 11942731]

[62]. Jaquins-Gerstl A, Shu Z, Zhang J, Liu Y, Weber SG, Michael AC, Effect of Dexamethasone on Gliosis, Ischemia, and Dopamine Extraction during Microdialysis Sampling in Brain Tissue, Analytical Chemistry83(20) (2011) 7662–7667. [PubMed: 21859125]

[63]. Woeppel KM, Zheng XS, Schulte ZM, Rosi NL, Cui XT, Nanoparticle Doped PEDOT for Enhanced Electrode Coatings and Drug Delivery, Advanced Healthcare Materials8(21) (2019) 1900622.

[64]. Kozai TDY, Li X, Bodily LM, Caparosa EM, Zenonos GA, Carlisle DL, Friedlander RM, Cui XT, Effects of caspase-1 knockout on chronic neural recording quality and longevity: Insight into cellular and molecular mechanisms of the reactive tissue response, Biomaterials35(36) (2014) 9620–9634. [PubMed: 25176060]

[65]. Kozai TDY, Gugel Z, Li X, Gilgunn PJ, Khilwani R, Ozdoganlar OB, Fedder GK, Weber DJ, Cui XT, Chronic tissue response to carboxymethyl cellulose based dissolvable insertion needle for ultra-small neural probes, Biomaterials35(34) (2014) 9255–9268. [PubMed: 25128375]

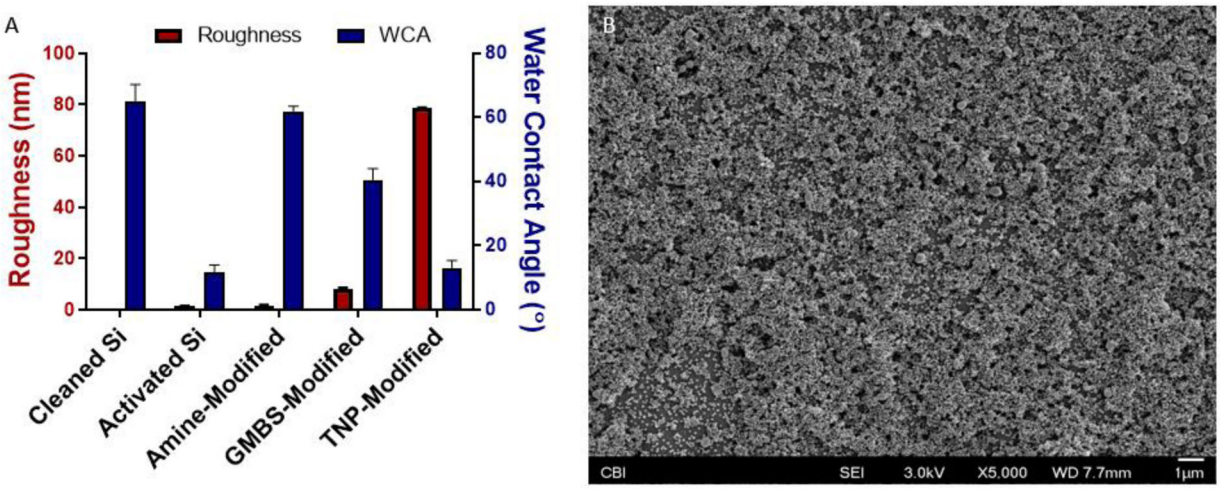

Figure 1.

Characterization of TNP modified substrates (A) water contact angle measurement changes during nanoparticle immobilization and surface roughness and changes in coating thickness of the modified silicon substrate measured by ellipsometry. Values represent change in thickness between steps. (B) SEM image of nanoparticle modified surface. Data presented as the mean ± standard error from nine trials.

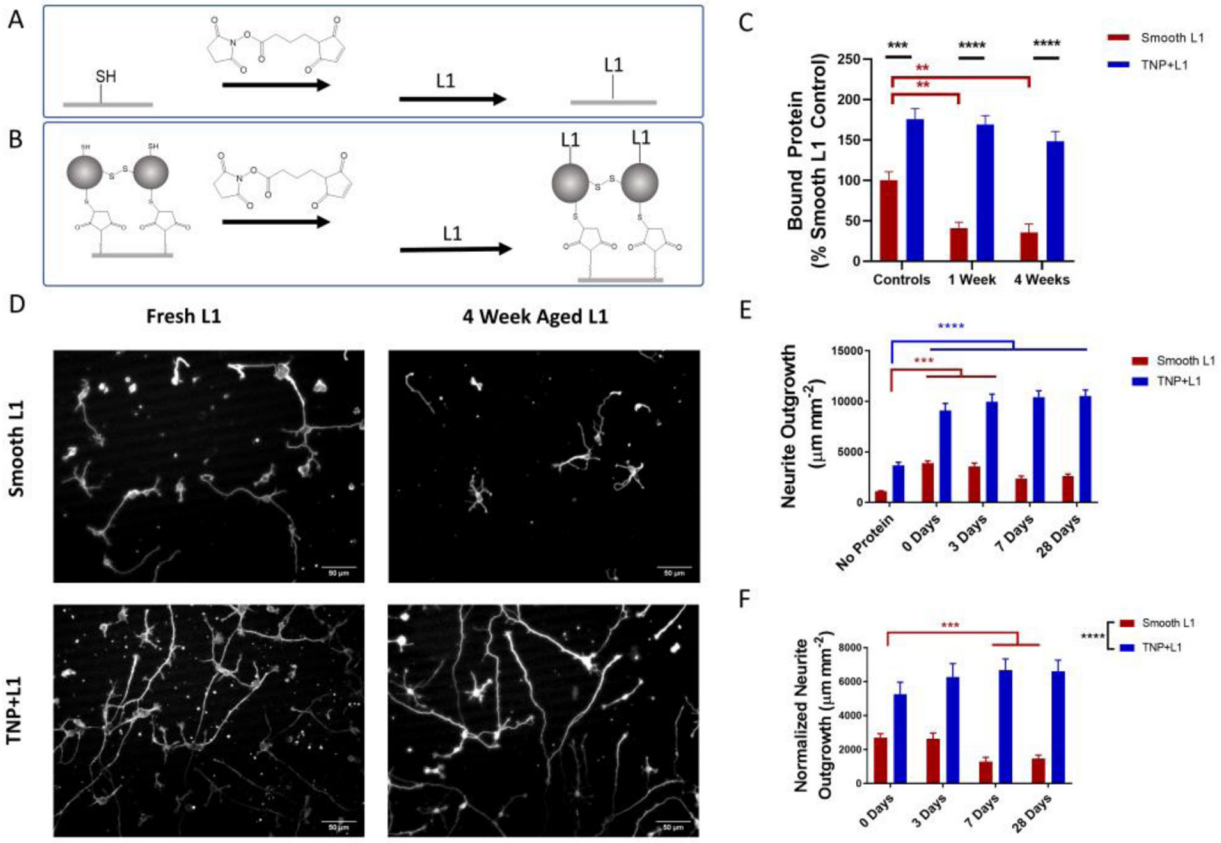

Figure 2.

Protein binding and bioactive lifetime A) Immobilization of L1 on MTS modified substrates via GMBS crosslinking. (B) Immobilization of L1 on TNP via GMBS crosslinking. Note that the binding mechanism of both MTS and TNP is identical. (C) Relative amounts of L1 bound to glass substrates after incubating for 7 or 28 days at 37°C in PBS, n=9 with significance between timepoints determined with one-way ANOVA with Tukey's post hoc. Significance between groups was determined with Student's t-test with a Bonferroni correction. (D) fluorescence images of b(III)-tubulin stained neuron cultures grown on freshly prepared L1 modified substrates and L1 modified substrates aged for 28 days. (E) Neurite outgrowth on smooth, rough, and protein modified substrates. (F) Quantified neurite outgrowth normalized to their respective non-protein modified surfaces. Data presented as the mean ± standard error from n=12 trials. Statistical significance was determined with a two-way ANOVA and Tukey's post hoc **p<0.01 ***p<0.001 ****p<0.0001.

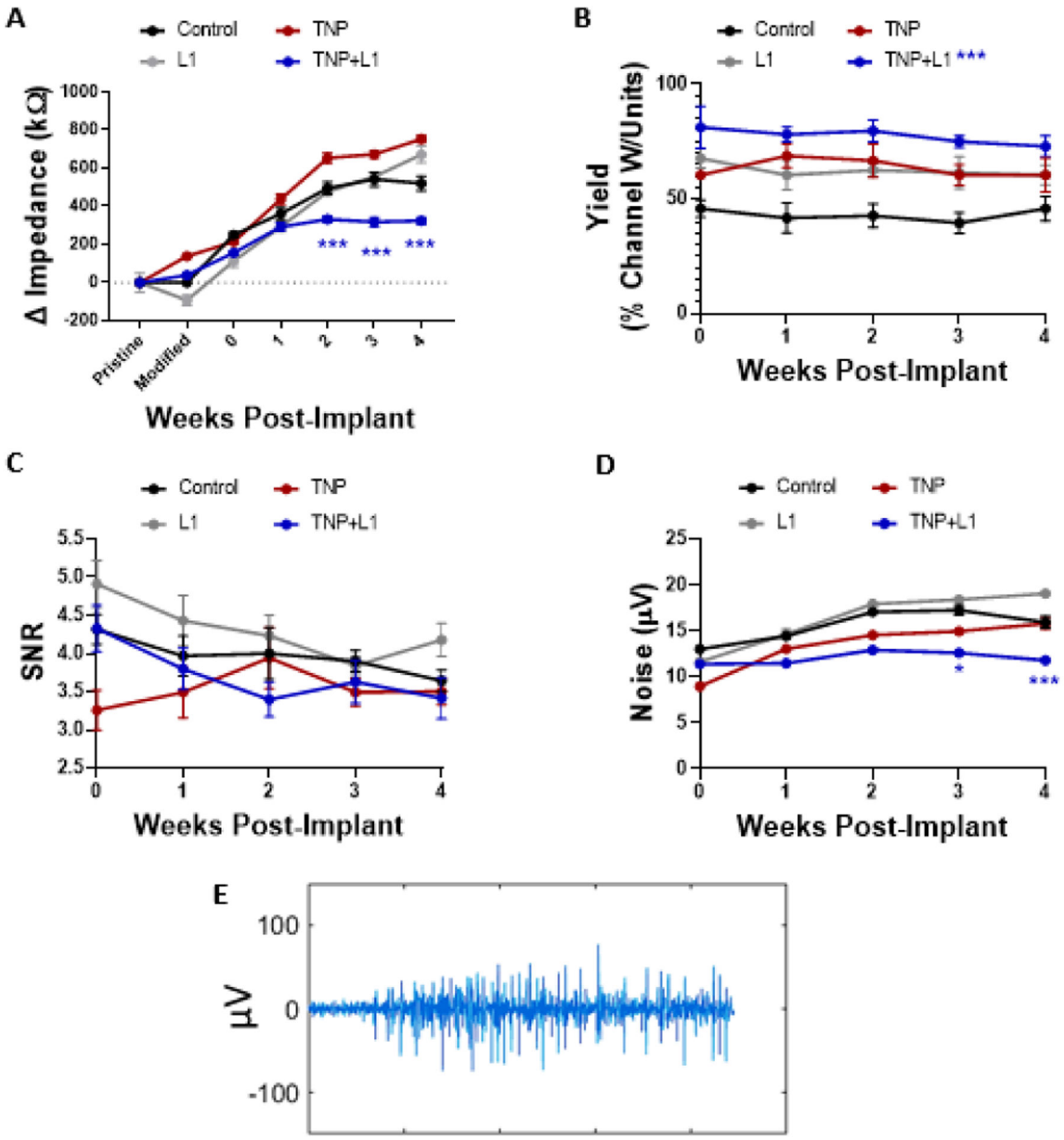

Figure 3.

Recording performance. (A) Impedance measurements normalized to the pristine electrode (before surface modification). The second data point indicates the change in impedance after modification. (B) Single unit yield (C) SNR, and (D) noise measured over the first four weeks of recording. When compared across all time points, yield (B) was significantly higher for the TNP+L1 modified electrodes. Data presented as the mean ± standard error from six animals (one probe with 16 electrode sites per animal) Significance was determined with two-way ANOVA with Tukey's post hoc *p<0.05, **p<0.01, ***p<0.001. (E) Sample neural recording traces from a TNP+L1 electrode after 4 weeks, filtered between 300 and 5,000Hz.

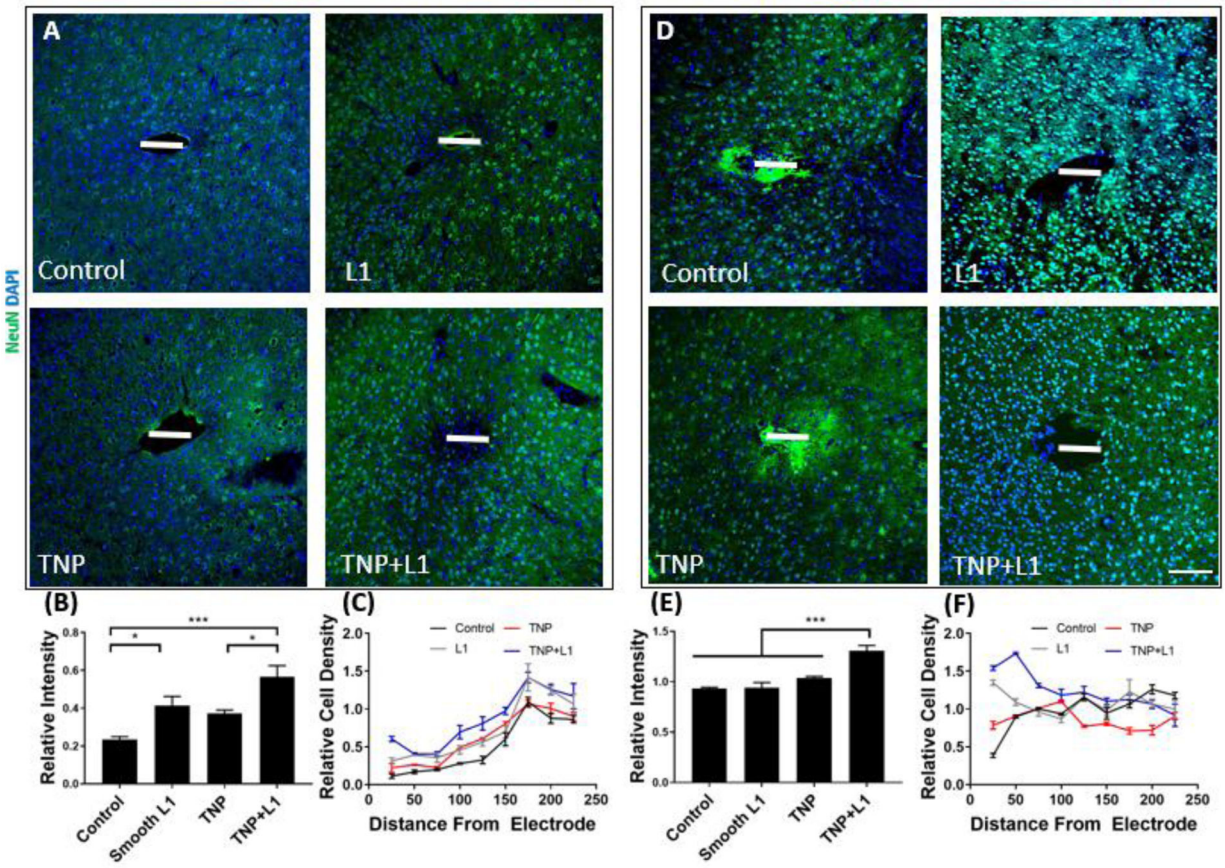

Figure 4.

Quantification of neural cell bodies. Values are scaled to contralateral tissues, where the relative intensity is 1. (A,D) Representative images of NeuN stained tissue slices after 1 week or 4 weeks of implantation, respectively. (B,E) Quantification of NeuN positive cells up to 100μm from the implant surface for 1- and 4-week implantation, respectively. (C,F) Relative cell density as a function of distance from the electrode for 1- and 4-week implants, respectively. Data presented as the mean ± standard error from four animals per timepoint. Significance was determined with one-way ANOVA with Tukey's post hoc *$p<0.05$ **$p<0.01$. Scale bar is 100μm

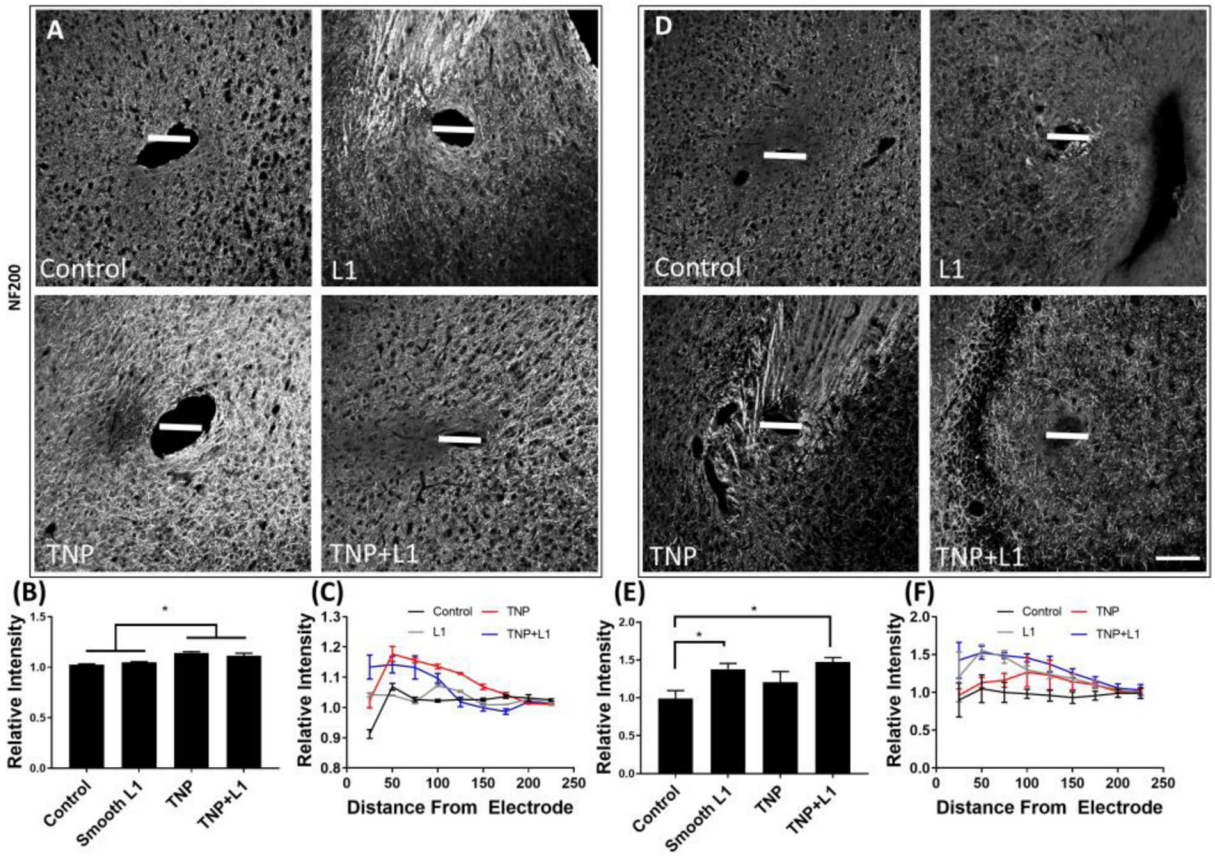

Figure 5.

Quantification of axons. Values are scaled to contralateral tissues, where the relative intensity is 1 (A,D) Representative images of NF-200 stained tissue slices after 1 week or 4 weeks of implantation, respectively. (B,E) Quantification of NF200 staining intensity up to 100μm from the implant surface for 1- and 4-week implantation, respectively. (C,F) Relative intensity as a function of distance from the electrode for 1- and 4-week implants, respectively. Data presented as the mean ± standard error from four animals per timepoint Significance was determined with one-way ANOVA with Tukey's post hoc *$p<0.05$. Scale bar is 100μm

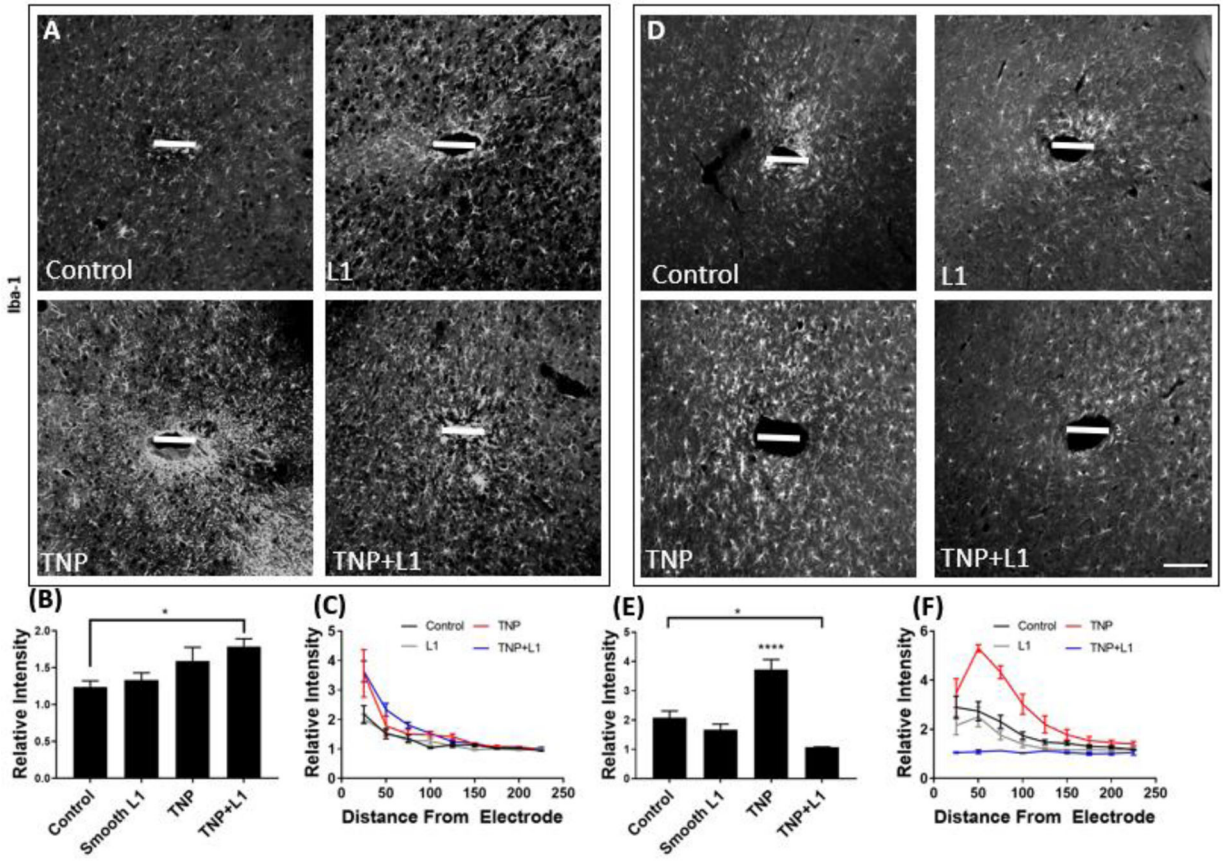

Figure 6.

Quantification of microglia. Values are scaled to contralateral tissues, where the relative intensity is 1 (A,D) Representative images of Iba-1 stained tissue slices after 1 week or 4 weeks of implantation, respectively. (B,E) Quantification of Iba-1 staining intensity up to 100μm from the implant surface for 1- and 4-week implantation, respectively. (C,F) Relative intensity as a function of distance from the electrode for 1- and 4-week implants, respectively. Data presented as the mean ± standard error from four animals per timepoint. Significance was determined with one-way ANOVA with Tukey's post hoc *$p<0.05$, ****$p<0.0001$. Scale bar is 100μm

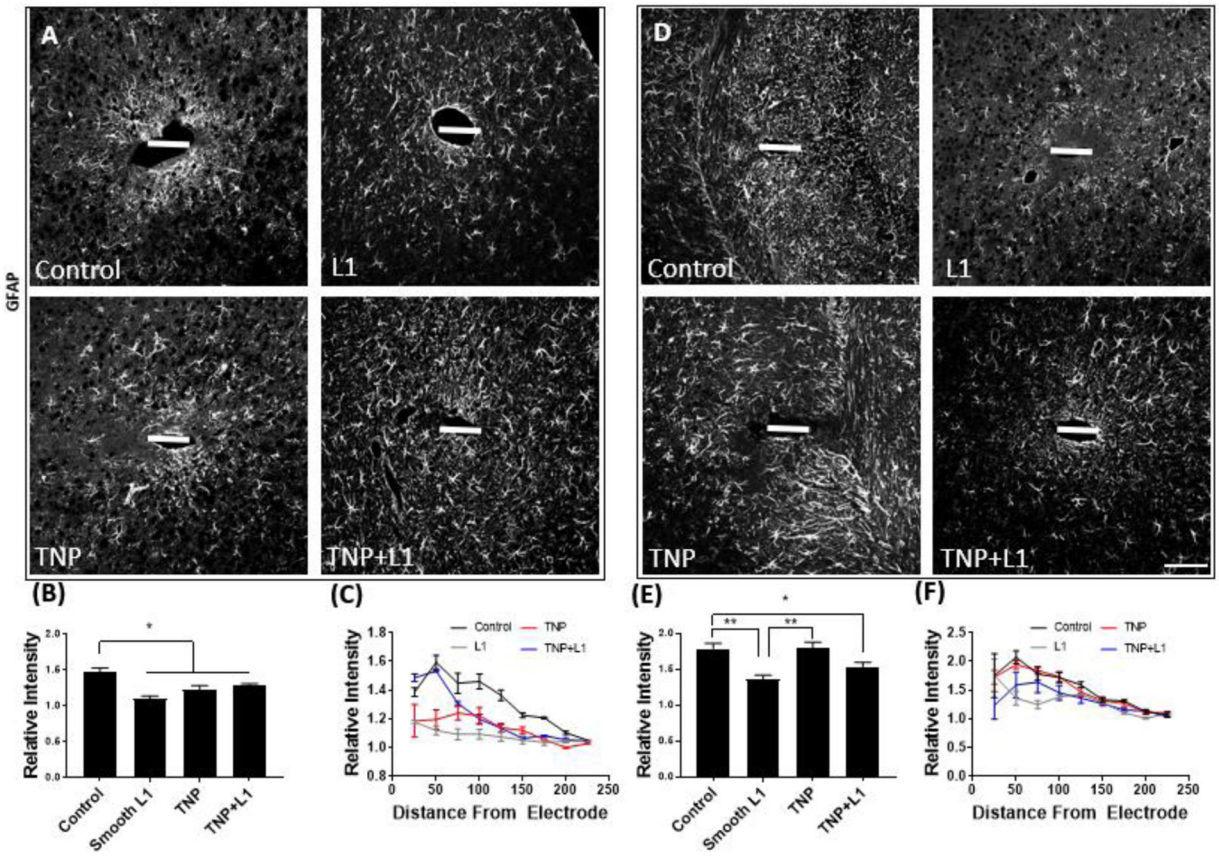

Figure 7.

Quantification of astrocytes. Values are scaled to contralateral tissues, where the relative intensity is 1 (A,D) Representative images of GFAP stained tissue slices after 1 week or 4 weeks of implantation, respectively. (B,E) Quantification of GFAP staining intensity up to 100μm from the implant surface for 1- and 4-week implantation, respectively. (C,F) Relative intensity as a function of distance from the electrode for 1- and 4-week implants, respectively. Data presented as the mean ± standard error from four animals per timepoint. Significance was determined with one-way ANOVA with Tukey's post hoc *$p<0.05$ **$p<0.01$. Scale bar is 100μm

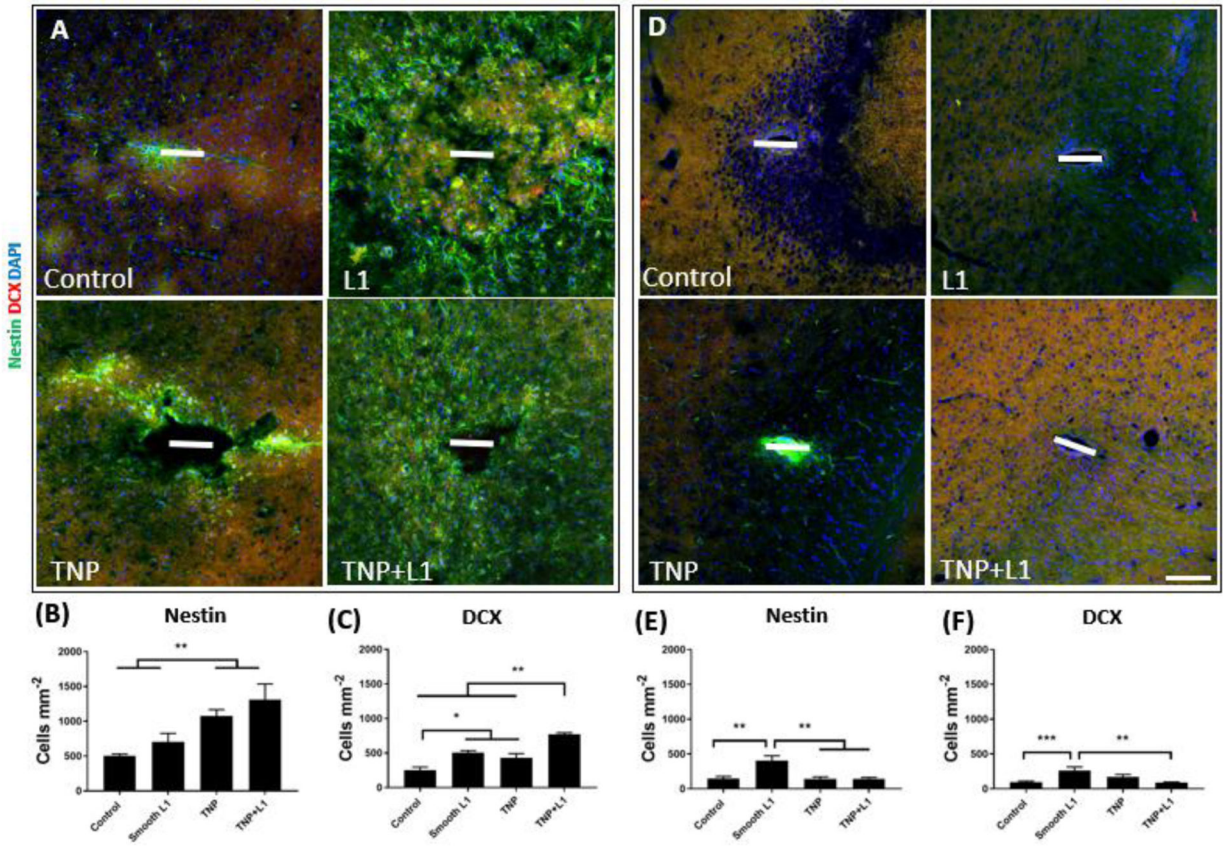

Figure 8.

Examination of the origin of local neurons. (A,D) Representative images of nestin (green) and DCX (red) stained tissue slices after 1 week or 4 weeks of implantation, respectively. (B,E) Quantification of nestin staining intensity up to 100μm from the implant surface for 1- and 4-week implantation, respectively. (C,F) Quantification of NDCX staining intensity up to 100μm from the implant surface for 1- and 4-week implantation, respectively. Data presented as the mean ± standard error from four animals per timepoint. Significance was determined with one-way ANOVA with Tukey's post hoc *p<0.05 **p<0.01, ***p<0.001. Scale bar is 100μm

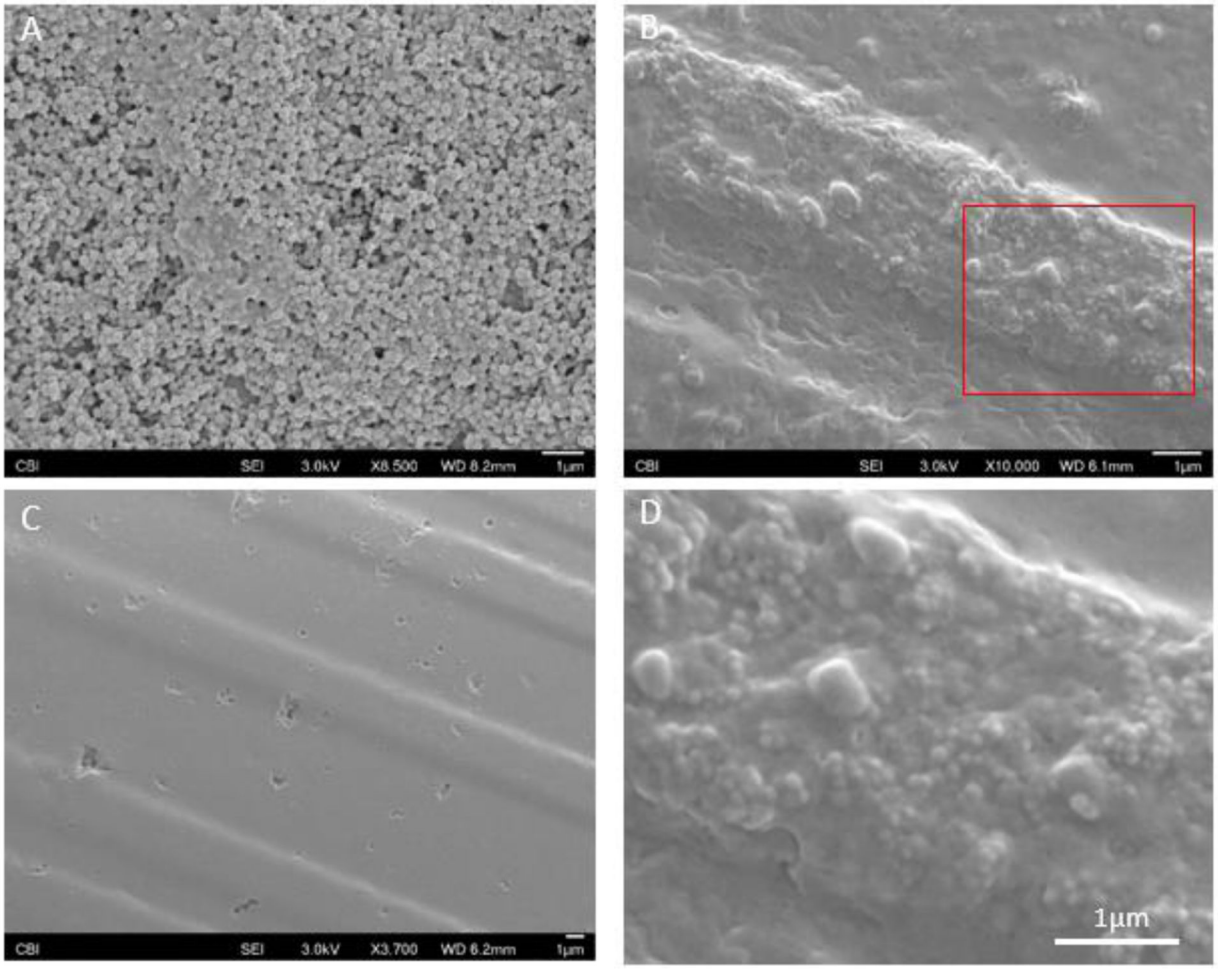

Figure 9.

Explant analysis. (A) SEM image of explanted nanoparticle modified electrode taken near the skull. (B) Nanoparticle modified electrode with biological materials attached. Nanoparticle topography can still be observed underneath the biological film. (C) Biofouling was also present on electrodes without TNP. (D) Enlarged region indicated by the red box in (B).

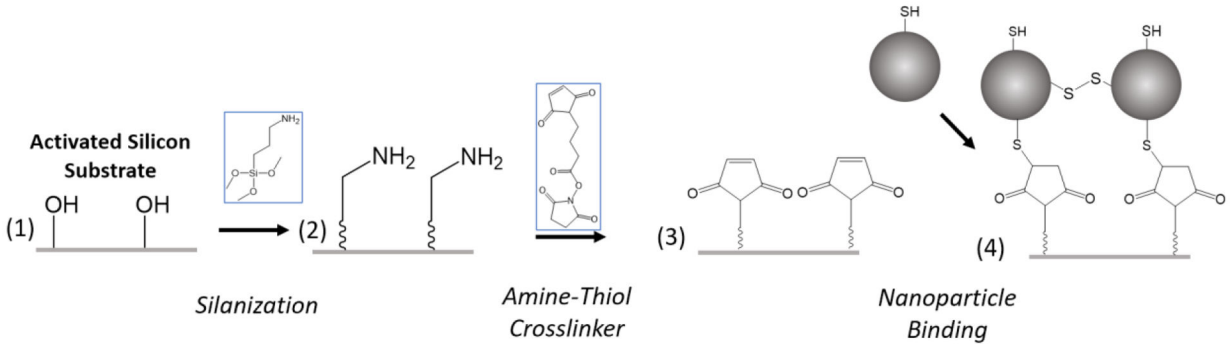

Scheme 1:

Nanoparticle immobilization. 1) Silicon substrates were first cleaned then activated with O2 plasma. 2) The activated substrate was then silanized with APTES, producing an amine functionalized surface. 3) The anime groups were then reacted with GMBS, displacing the oxy-succinimide group, leaving the maleimide group. 4) TNP were then bound to the maleimide group via thiol-ene click chemistry. Additional bonds between TNP may form via disulfide bridging.

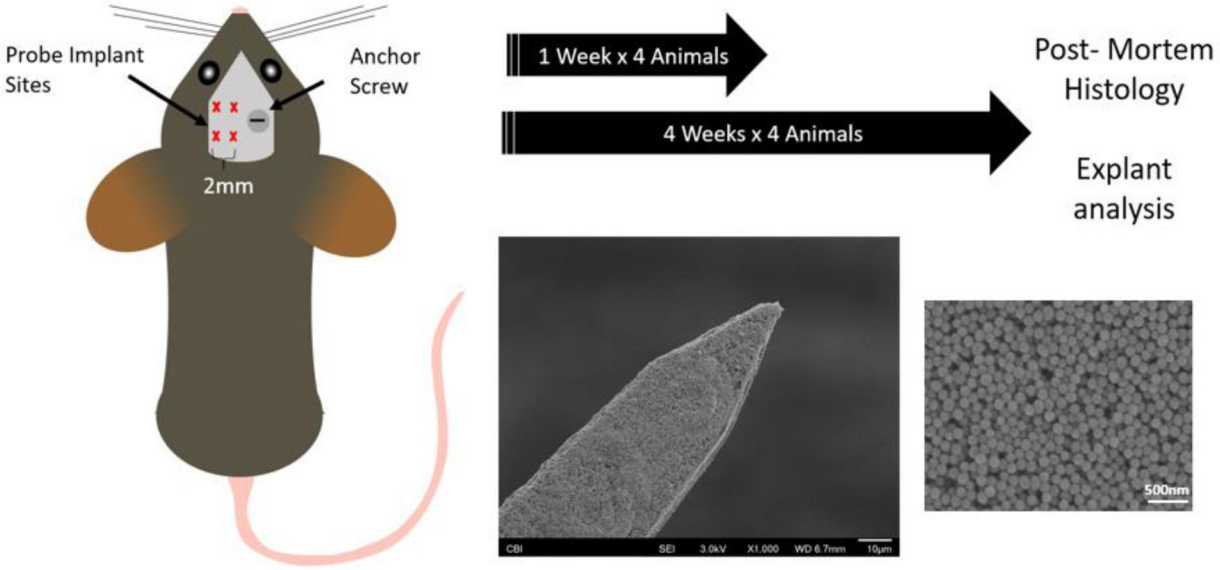

Scheme 2.

In vivo histology experimental setup. Mice were implanted with 4 probes consisting of a control, unmodified electrode, an L1 modified electrode, a TNP modified electrode, and a TNP+L1 modified electrode. An anchor screw was placed over the right hemisphere to aid in stabilizing the dental cement headcap. Animals were then perfused at 1- or 4-weeks post implantation. Brain tissue was collected for immunostaining, while the explanted electrodes were examined under SEM. Included is a pre-implant SEM image of a TNP modified electrode and a high magnification image of the same electrode